

1 Concurrent photochemical whitening and darkening of ambient 2 brown carbon

3 Qian Li¹, Dantong Liu^{1*}, Xiaotong Jiang¹, Ping Tian², Yangzhou Wu¹, Siyuan Li¹, Kang Hu¹, Quan Liu³,
4 Mengyu Huang², Ruijie Li², Kai Bi², Shaofei Kong⁴, Deping Ding²

5 ¹Department of Atmospheric Science, School of Earth Science, Zhejiang University, Hangzhou, 310027, China

6 ²Beijing Key Laboratory of Cloud, Precipitation and Atmospheric Water Resources, Beijing Meteorological Service, Beijing,
7 100089, China.

8 ³State Key Laboratory of Severe Weather & Key Laboratory of Atmospheric Chemistry of CMA, Chinese Academy of
9 Meteorological Sciences, Beijing, 100081, China

10 ⁴Department of Atmospheric Science, School of Environmental Science, China University of Geosciences, Wuhan, 430074,
11 China

12 *Correspondence to:* Dantong Liu (dantongliu@zju.edu.cn)

13 **Abstract.** The light-absorbing organic aerosol (OA), known as brown carbon (BrC), has important radiative impacts, however
14 its sources and evolution after emission remain to be elucidated. In this study, the light absorption at multiple wavelengths,
15 mass spectra of OA and microphysical properties of black carbon (BC) were characterized at a typical sub-urban environment
16 in Beijing. The absorption of BC is constrained by its size distribution and mixing state and the BrC absorption is obtained by
17 subtracting the BC absorption from the total aerosol absorption. Aerosol absorption was further apportioned to BC, primary
18 BrC and secondary BrC by applying the least-correlation between secondary BrC and BC. The multi-linear regression analysis
19 on the factorized OA mass spectra indicated the OA from traffic and biomass burning emission contributed to primary BrC.
20 Importantly, the moderately oxygenated OA (O/C=0.62) was revealed to highly correlate with secondary BrC. These OA had
21 higher nitrogen content, in line with the nitrogen-containing functional groups detected by the Fourier transform infrared
22 spectrometer. The photochemical processes were found to reduce the mass absorption cross section (MAC) of primary OA but
23 enhancement for secondary OA, resulting in the contribution of primary BrC to total absorbance decreased about 20% but
24 enhanced contribution of secondary BrC by 30%, implying the concurrent whitening and darkening of BrC. This provides field
25 evidence that the photochemically produced secondary nitrogen-containing OA can considerably compensate some bleaching
26 effect on the primary BrC, hereby causing radiative impacts.

27 1. Introduction

28 Atmospheric absorbing organic aerosol (OA), known as brown carbon (BrC), is an important contributor to anthropogenic
29 absorption besides black carbon (BC) (Laskin et al., 2015; Liu et al., 2020), particularly at shorter visible wavelengths (Bahadur
30 et al., 2012). Due to complex compositions of OA, the primary sources and subsequent evolution of BrC in the atmosphere
31 remains to be explicitly understood and causes uncertainties in evaluating the radiative impacts of BrC (Liu et al., 2020).

32 The chromophores of BrC are mainly aromatic compounds associated with certain functional groups (Liu et al., 2015c).
33 Particularly, compounds containing nitro, nitrated or other forms of nitrogen-containing functional groups are more absorbing
34 (Nakayama et al., 2013; Jacobson, 1999). It is well established that primary OA, especially from biomass burning, contains a
35 large fraction of BrC (Andreae and Crutzen, 1997; Rizzo et al., 2013; Bond, 2001). These primary BrC has a range of
36 absorptivity, which was found to be controlled by burning phases. OA co-emitting with BC (the flaming phase) exhibited a
37 higher absorptivity than OA-dominated smoldering phase (Liu et al., 2021). BrC can experience reactions with atmospheric
38 oxidants after emission. Previous studies (Satish et al., 2017; Satish and Rastogi, 2019; Dasari et al., 2019) found nitrogenous
39 compounds from biomass burning were responsible for BrC over South Asia and the chromophores were photobleached in the
40 afternoon. Numerous field and laboratory studies found the decrease of BrC absorptivity due to photobleaching of
41 chromophores, with lifetime ranging from a few hours (Zhao et al., 2015; Liu et al., 2021) to a few days (Forrister et al., 2015),
42 which may depend on the concentration of ambient hydroxyl radical (Wang et al., 2014), also influenced by relative humidity
43 and particle volatility (Schnitzler et al., 2020). The absorptivity of BrC could be also enhanced due to addition of functional
44 groups by forming conjugated structure with aromatics. This was supported by a number of laboratory studies that BrC
45 absorptivity could be enhanced when forming nitrogen-containing organic compounds, such as the formation of nitro-
46 aromatics when aromatics reacted with NO_x (Nakayama et al., 2013), or produced organic amine after reacting with ammonia
47 (Updyke et al., 2012). The enhancement of BrC absorptivity could occur either through nitration of existing chromophores, or
48 formation of new secondary organic aerosol (SOA) chromophores through gas-phase oxidation.

49 The above findings mean the enhancement or bleaching of BrC absorptivity via photooxidation will coexist. The time scale
50 between both competing processes will ultimately determine the lifetime of BrC in the atmosphere. However, both processes
51 have been rarely investigated in the field to explicitly determine the BrC components which principally determine the
52 respective enhancement or decrease of its absorptivity, particularly in regions influenced by combined anthropogenic sources.
53 In this study, by measurements using multiple-wavelength absorption and microphysical properties of BC in a sub-urban region,
54 the absorption of BC, primary and secondary BrC was discriminated. In conjunction with source attribution via OA mass
55 spectra, we are able to link the segregated absorption with certain sources and investigate their primary information and
56 subsequent evolution. The competition between photobleaching and secondary formation of BrC was investigated in real world.

57 2. Experimental and instrumentation

58 2.1 Site description and meteorology

59 The experiment was conducted during springtime at the Beijing Cloud Laboratory and Observational Utilities Deployment
60 Base (117.12°E, 40.14°N), which is located in the northeast suburban area in Beijing (Fig S1a). The site is surrounded by the
61 northwest mountain ridge, without significant local primary anthropogenic emissions (Hu et al., 2021). The 72-h backward
62 trajectories with every 3 hours initializing from the site are analyzed by the HYSPLIT model (Draxier and Hess, 1998) using
63 the 3-hourly 1°×1° meteorological field from the GDAS reanalysis product. The obtained backward trajectories were further
64 clustered to group the similar transport pathways (Makra et al., 2011). The meteorological parameters, including the
65 temperature (T), ambient relative humidity (RH), wind speed (WS) and wind direction (WD) were measured by a monitoring
66 station on the site.

67 2.2 Measurements of BC microphysics and absorption coefficient

68 In this study, the ambient aerosols were sampled by a large-flow (1.05 m³ min⁻¹) air particle sampler (TH-1000C II) with a
69 PM_{2.5} impactor (BGI SCC 1.829) and dried by a silica drier before measurement. The single particle soot photometer (SP2,
70 DMT., USA) used continuous laser at $\lambda=1064$ nm to incandesce light-absorbing aerosols (such as BC) for irradiating detectable
71 visible light. The incandescence signal was used to measure the refractory black carbon (rBC) mass. The SP2 incandescence
72 signal was calibrated using the Aquadag standard (Acheson Inc., USA), and a factor of 0.75 was applied to correct for ambient
73 BC (Laborde et al., 2012). The scattering signal was calibrated by monodispersed polystyrene latex spheres (PSL). The BC
74 core diameter (D_c) was calculated from the measured BC mass by assuming a BC density of 1.8 g cm⁻³ (Bond and Bergstrom,
75 2006). The leading edge only (LEO) method was applied to reconstruct the scattering signal of BC, which was used to
76 determine the coated particle diameter (D_p) by a Mie-lookup table with the inputs of scattering and incandescence signal of
77 each BC particle (Liu et al., 2014; Taylor et al., 2015). The mass median diameter (MMD) is derived from the D_c distribution,
78 which is determined as below and above MMD the rBC mass concentration is equal (Liu et al., 2019a). The bulk coating
79 thickness (D_p/D_c) is calculated as the cubic root of ratio of the total coated BC volume divided by the total volume of rBC.

80 The mass absorption cross section (MAC) (in m² g⁻¹) of each BC particle can be calculated using the measured coated and
81 uncoated BC sizes by applying the Mie core-shell calculation. The absorption coefficient of BC at certain wavelength, $\sigma_{\text{abs,BC}}$
82 (λ) is determined by multiplying the calculated MAC and rBC mass concentration at each size:

$$83 \sigma_{\text{abs,BC}}(\lambda) = \sum_i \text{MAC}(\lambda, D_{p,i}, D_{c,i}) m(\log D_{c,i}) \Delta \log D_{c,i} \quad (1)$$

84 where $m(\log D_{c,i})$ denotes the BC mass concentration at each logarithmic bin of D_c . The SP2 measurement at $\lambda=1064$ nm longer
85 than mostly populated BC size means the derived coatings and subsequent calculation of MAC is relatively independent of
86 particle shape within uncertainty of 21% (Liu et al., 2014; Hu et al., 2021).

87 The absorption coefficients at wavelengths $\lambda= 375, 470, 528, 635$ and 880 nm were measured by a Micro-Aethalometer
88 (MA200, Aethlabs, San Francisco, CA, USA). Aerosol particles were collected on filter tapes, on which the light attenuation
89 was measured continuously with a time resolution of 30 s. The loading effect of filters was automatically corrected by

90 measuring attenuation at two different sampling flow rates on two spots in parallel (Drinovec et al., 2015a). Moreover, a multi-
91 scattering correction factor (C-value) of 3.5, 3.2 and 2.4 at the wavelengths 370 nm, 528 nm and 880 nm, respectively were
92 utilized to correct attenuation for the multiple light scattering effect. It was obtained by comparing the absorption coefficient
93 with a photoacoustic soot spectrometer (PASS-3, DMT) (Hu et al., 2021).

94 2.3 Attribution of primary and secondary BrC absorption coefficient

95 The absorption coefficient of BC at different λ is calculated using the measured uncoated core and coated size as mentioned
96 above. The absorption coefficient of total BrC is obtained by subtracting the BC absorption coefficient from the total absorption
97 at certain wavelength, expressed as:

$$98 \sigma_{\text{abs, BrC}}(\lambda) = \sigma_{\text{abs, total}}(\lambda) - \sigma_{\text{abs, BC}}(\lambda) \quad (2)$$

99 where the absorption coefficient of BC ($\sigma_{\text{abs, BC}}$) is obtained from the SP2 measurement, $\sigma_{\text{abs, total}}(\lambda)$ is the total light absorption
100 of aerosols measured by the MA200. The absorption coefficient of secondary BrC, the absorption not contributed by primary
101 sources, is obtained by subtracting the absorption of all primary sources from the total absorption (Crilley et al., 2015),
102 expressed as:

$$103 \sigma_{\text{abs, secBrC}}(\lambda) = \sigma_{\text{abs, total}}(\lambda) - \sigma_{\text{abs, pri}}(\lambda) \quad (3)$$

104 where $\sigma_{\text{abs, pri}}(\lambda)$ is the light absorption from primary sources. Here an assumption is made that light absorption from primary
105 aerosols is all from combustion sources, and these sources necessarily contain BC (Wang et al., 2018a). Therefore, the total
106 absorption from primary sources can be obtained by scaling a factor from the mass concentration of BC, expressed as:

$$107 \sigma_{\text{abs, pri}}(\lambda) = \left(\frac{\sigma_{\text{abs, total}}}{[\text{rBC}]} \right)_{\text{pri}} \cdot [\text{rBC}] \quad (4)$$

108 where [rBC] is the mass concentration of rBC measured by the SP2, $\left(\frac{\sigma_{\text{abs, total}}}{[\text{rBC}]} \right)_{\text{pri}}$ is the scaling factor to derive the absorption
109 of primary combustion sources from [rBC]. This factor is obtained using the minimum R-squared (MRS) approach (Wu and
110 Yu, 2016), by adjusting the factor until a minimum correlation between $\sigma_{\text{abs, secBrC}}$ and [rBC] is reached because the absorption
111 from secondary sources are least likely to covary with that from primary sources (Wang et al., 2019a). This method has been
112 used in urban and sub-urban environment to obtain the primary BrC associated with combustion sources. Being different from
113 previous studies, an auxiliary characterization of rBC mass measured by the SP2 is used here to avoid the possible interference
114 from absorption measured by the same instrument. There may be different $\left(\frac{\sigma_{\text{abs, total}}}{[\text{rBC}]} \right)_{\text{pri}}$ ratio between traffic and biomass

115 burning sources and this may lead to bias in deriving the subsequent results. We have more carefully investigated the diurnal
116 pattern of hydrocarbon-like OA (HOA) and biomass burning OA (BBOA), and found only a slight morning rush-hour peak
117 for HOA (though bearing considerable variation). A further investigation on the HOA/BBOA ratio found no apparent diurnal
118 pattern (bearing large variation), shown in Fig. S8. The source difference is therefore not considered to have significantly
119 influenced the diurnal pattern of derived parameters. In addition, this method is only valid with sufficient data points thus we

120 may only obtain a single mean value for the entire experiment, which represents the mean $\left(\frac{\sigma_{abs,total}}{[rBC]}\right)_{pri}$ in this environment
 121 during the experimental period. Previous studies using this method also derived the mean value of $\left(\frac{\sigma_{abs,total}}{[rBC]}\right)_{pri}$ for the urban
 122 environment influenced by multiple sources including traffic, coal combustion and biomass burning (Wang et al., 2019c; Wang
 123 et al., 2020; Gao et al., 2022). The $\left(\frac{\sigma_{abs,total}}{[rBC]}\right)_{pri}$ ratio at $\lambda=375$ nm, 470 nm, 528 nm, 635 nm and 880 nm is calculated to be
 124 20.7, 17.0, 14.4, 11.7 and 5, respectively (Fig. S2), which falls within the reported values from previous studies 11-50 (Zhang
 125 et al., 2020; Wang et al., 2019a). This scenario assumes a relatively consistent absorption relative to BC mass concentration
 126 from sources during experiment. This however may not include some sporadic events when sources with distinct OA or BC
 127 mass fraction may be introduced and alter the single $\left(\frac{\sigma_{abs,total}}{[rBC]}\right)_{pri}$ ratio. The $\sigma_{abs,secBrC}$ therefore represents the overall mean
 128 value during the experimental period but this ratio will vary with seasons and locations. The σ_{abs} of primary BrC can then be
 129 calculated as:

$$130 \sigma_{abs,priBrC}(\lambda) = \sigma_{abs,BrC}(\lambda) - \sigma_{abs,secBrC}(\lambda) \quad (5)$$

131 where $\sigma_{abs,BrC}$ and $\sigma_{abs,secBrC}$ is calculated from Equation (2) and (3), respectively.

132 2.4 Composition measurement

133 The mass concentration and chemical composition of non-refractory sub-micron PM (NR-PM₁) including organic aerosols
 134 (OA), nitrate (NO₃⁻), sulfate (SO₄²⁻), chloride (Cl⁻) and ammonium (NH₄⁺) were determined with a High-Resolution Time-of-
 135 Flight Aerosol Mass Spectrometer (HR-ToF-AMS, Aerodyne Research Inc., USA). The setup, operation, and calibration
 136 procedures of the AMS have been described elsewhere (Canagaratna et al., 2007). During this field observation, the AMS was
 137 operated in V-mode for the quantification of mass concentrations. The composition-dependent collection efficiencies were
 138 applied ((Middlebrook et al., 2012), and the ionization efficiency was calibrated using 300 nm pure ammonium nitrate (Jayne
 139 et al., 2000). Elemental ratios of OA including oxygen-to-carbon (O/C), hydrogen-to-carbon (H/C) and nitrogen-to-carbon
 140 (N/C) were determined to the improved-ambient method (Canagaratna et al., 2015).

141 Positive Matrix Factorization (PMF) (Paatero and Tapper, 1994) was performed on the inorganic and organic high-resolution
 142 mass spectra to distinguish OA components from different sources (Zhang et al., 2011; Ulbrich et al., 2009; Decarlo et al.,
 143 2010). The mass spectra of the combined matrix for $m/z < 120$ were excluded in PMF analysis. Five OA factors were identified.
 144 The diagnostics of PMF is summarized in Text S1 and Fig. S6.

145 2.5 Offline Fourier transform infrared spectrometer (FTIR) analysis

146 Particulate Matter (PM) samples were collected once a day onto prebaked (600°C, 4h) quartz fiber filters (Whatman, QMA,
 147 USA) using a large-flow (1.05 m³ min⁻¹) air particle sampler (TH-1000C II). The collected filter samples were stored in the

148 refrigerator at -20°C before analysis. The infrared spectra of collected samples were measured by a Fourier transform infrared
149 spectrometer (FTIR, Thermo Scientific, USA) equipped with an iD5 attenuated total reflectance accessory (diamond crystal)
150 to quantify the chemical functional groups over the wavenumbers range of $550\text{-}4000\text{ cm}^{-1}$ with a resolution of 0.5 cm^{-1} . The
151 NO and NO₂ symmetric stretch in the FTIR spectra can characterize the functional groups associated with nitrogen-containing
152 organics (Coury and Dillner, 2008). Fig. S3 shows typical examples of FTIR spectra and the assigned functional groups for
153 the three pollution levels during experiment. The peak at 1110 cm^{-1} corresponds to the background of the quartz fiber filter
154 overlapped with some X-H bending vibrations, which is subtracted for the following analysis. The characteristic organic nitrate
155 spectra appear at wavenumbers 860 cm^{-1} (NO symmetric stretch), 1280 cm^{-1} (NO₂ symmetric stretch) and $1630\text{-}1640\text{ cm}^{-1}$
156 (NO₂ asymmetric stretch) (Bruns et al., 2010). After baseline calibration, The FTIR peaks of 1630 cm^{-1} and 860 cm^{-1} are
157 integrated the absorption areas above the baseline. The summed integrated area of -NO and -NO₂ are hereby used to indicate
158 the nitrogen-containing organics. There was no discernable peak of carbonyl group for our infrared spectrum, and the peak of
159 OH at 2500 cm^{-1} - 3400 cm^{-1} for the carboxylic acid is not discernable neither, thus the influence of ketone and carboxylic acid
160 may be of less importance for our dataset.

161 3. Results and Discussion

162 3.1 Source attributed OA

163 The overview results are shown in Fig. S1. The organics dominated the aerosol compositions for most time, but occasionally
164 nitrate was the most abundant component (Fig. S1g). Note that the nitrate here may also include components containing in
165 organics besides ammonium nitrate. Backward trajectories (Fig. S1a-d) showed that the most abundant PM₁ concentration was
166 associated with air masses transported in shorter distance from southern regions (C1), but the longer and faster northerly
167 transported air mass from cleaner north (C2) could dilute the concentrations.

168 The resolved OA factors by the PMF analysis are shown in Fig. 1, including the mass spectra, time series and diurnal profiles
169 of each PMF factor with corresponded external and internal tracers. Three primary OA (POA) were identified as HOA,
170 cooking-related OA (COA), BBOA, with O/C of 0.31, 0.18 and 0.39 respectively. These POA had considerable fraction of
171 hydrocarbon fragments (C_xH_y), indicating their less aged status. The HOA profile was characterized by higher contributions
172 of aliphatic hydrocarbons and has dominated ion tracers such as m/z 41 (C₃H₅⁺), 43 (C₃H₇⁺), 55 (C₄H₇⁺) and 57 (C₄H₉⁺). The
173 HOA concentration correlated with BC ($r=0.62$), which emits from traffic emissions. The diurnal variation exhibited strong
174 morning and afternoon rush-hour peaks of mass concentration. This factor was consistent with the mass spectra of previously
175 measured HOA from on-road vehicle emissions in urban cities (Zhang et al., 2005; Aiken et al., 2009; Sun et al., 2016; Hu et
176 al., 2017), which has m/z peaks characteristic of hydrocarbon fragments in series of C_nH_{2n+1}⁺ and C_nH_{2n-1}⁺. The mass spectrum
177 of HOA shows overall similarity to those of primary OA emitted from gasoline and diesel combustion sources ($r=0.68$) (Elser
178 et al., 2016).

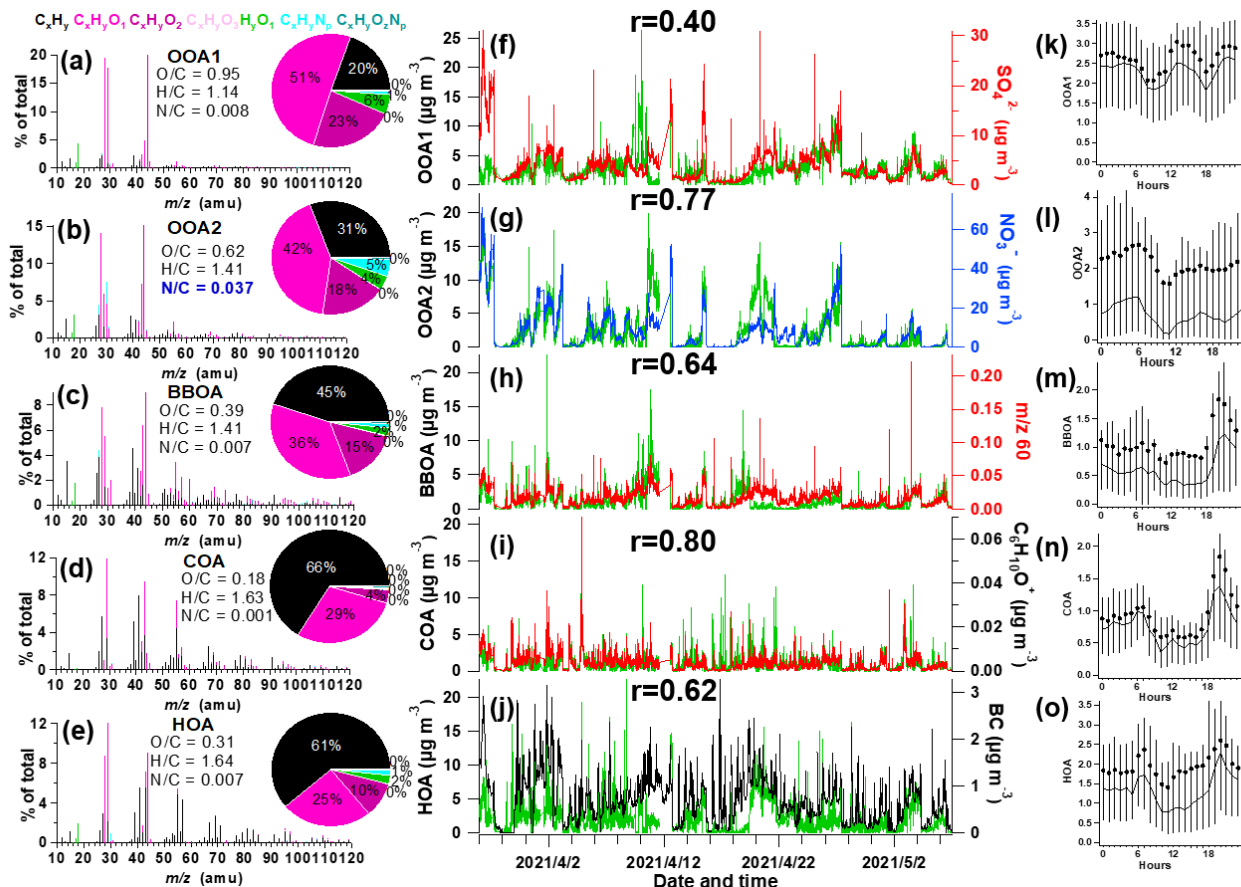
179 The OA from cooking sources (COA) is also characterized by prominent hydrocarbon ion series, however, with higher signal
180 at $C_nH_{2n-1}^+$ than $C_nH_{2n+1}^+$. COA had apparent fragments of both $C_4H_9^+$ and $C_3H_3O^+$, and has a higher ratio of $C_3H_3O^+/C_3H_5O^+$
181 (3.1), $C_4H_7^+/C_4H_9^+$ (2.2) than HOA (0.9–1.1), with cooking-related fragments of $C_5H_8O^+$ (m/z 84), $C_6H_{10}O^+$ (m/z 98) and
182 $C_7H_{12}O^+$ (m/z 112) (Sun et al., 2011b; Mohr et al., 2012). The COA shows overall similar spectral pattern to the reference
183 spectra of COA ($r=0.92$) (Elser et al., 2016). Its minor peak at noon and larger peak in the evening (Fig. 11) also corresponded
184 with the lunch and dinner time respectively. There was only a minor peak at noon for COA, which may be due to the sub-urban
185 nature of the site where the major aerosols from cooking sources may have been processed and lost the signature near source.
186 The feature of this factor was also observed in sub-urban environment (Huang et al., 2021).

187 The BBOA factor was identified based on the prominent signals of m/z 60 ($C_2H_4O_2^+$) and 73($C_3H_5O_2^+$), which are known
188 fragments of levoglucosan (Cubison et al., 2011). And BBOA also correlated with potassium (K^+ , $r = 0.80$), which are indicator
189 of biomass burning (Pachon et al., 2013; Brown et al., 2016). The m/z 60 and 73 together with a unique diurnal variation have
190 been shown to be a robust marker for the presence of aerosols from biomass burning emissions in many urban locations (Sun
191 et al., 2016). The BBOA shows very similar mass spectral patterns to previously reported reference spectra of biomass burning
192 ($r=0.94$) (Elser et al., 2016). The BBOA factor that was identified in spring accounted for 12.8% of the total OA in Beijing,
193 similar to previous reports (Hu et al., 2017). Biomass (Cheng et al., 2013) and solid fuel burning emissions (Sun et al., 2014)
194 have been widely observed to importantly contribute to the primary OA in this region. This off-road combustion source was
195 particularly abundant during wintertime for residential heating activities (Shen et al., 2019; Yang et al., 2018; Liu et al., 2016),
196 while boiler for industry use (mostly using coal as fuel) was in operation throughout the year (Liu et al., 2015b). During the
197 springtime of the experiment, the residential heating activities dropped due to increased ambient temperature thus the BBOA
198 may be mainly contributed by the industry sector.

199 Two types of oxygenated organic aerosols (OOA) were identified, in moderate (OOA2, $O/C=0.62$) and high oxidation state
200 (OOA1, $O/C=0.95$), respectively, which is very similar to the spectra of OOA factors resolved in other cities (Hayes et al.,
201 2013; Ulbrich et al., 2009). The average mass spectrum of OOA2 in this study is characterized by m/z 29 (mainly CHO^+), 43
202 (mainly $C_2H_3O^+$) and m/z 44 (CO_2^+), similar to the semi-volatile OOA spectrum identified in other locations (Sun et al., 2011a;
203 Zhou et al., 2016). On average, OOA2 accounts for 42% and 18% of $C_xH_yO^+$ and $C_xH_yO_2^+$ ions, respectively (Fig. 1b). These
204 results clearly indicate that OOA2 was primarily composed of less oxygenated, possibly freshly oxidized organics. Notably,
205 OOA2 had a substantially higher N/C than other factors ($N/C=0.037$), and had highest correlation with nitrate ($r=0.77$) and
206 with $C_xH_yN_z$ and $C_xH_yN_zO_p$ fragments ($r=0.83$). This factor therefore tends to largely result from nitrogen-containing OA and
207 its elevation at night may be also associated with dark oxidation by nitrate radical.

208 The mass spectrum of OOA1, which was characterized by a dominant peak at m/z 44 (mainly CO_2^+), a highest O/C (0.95). On
209 average, OOA1 contributes 51% of the $C_xH_yO^+$ signal and 23% of the $C_xH_yO_2^+$ signal (Fig. 1a). OOA1 showed particularly
210 high correlation with sulfate ($r=0.40$) because of their similar volatilities (Huffman et al., 2009; Jimenez et al., 2009). The
211 slight enhancement at noon for OOA1 (also for OOA2) soon after morning rush-hour indicated the likely rapid formation of
212 SOA through photooxidation. This significantly higher mean OOA2 than median value in the diurnal pattern indicated that

213 this OA type was largely associated with pollution events. Both OOA1 and OOA2 showed nighttime peak maybe due to
 214 reduced boundary layer.

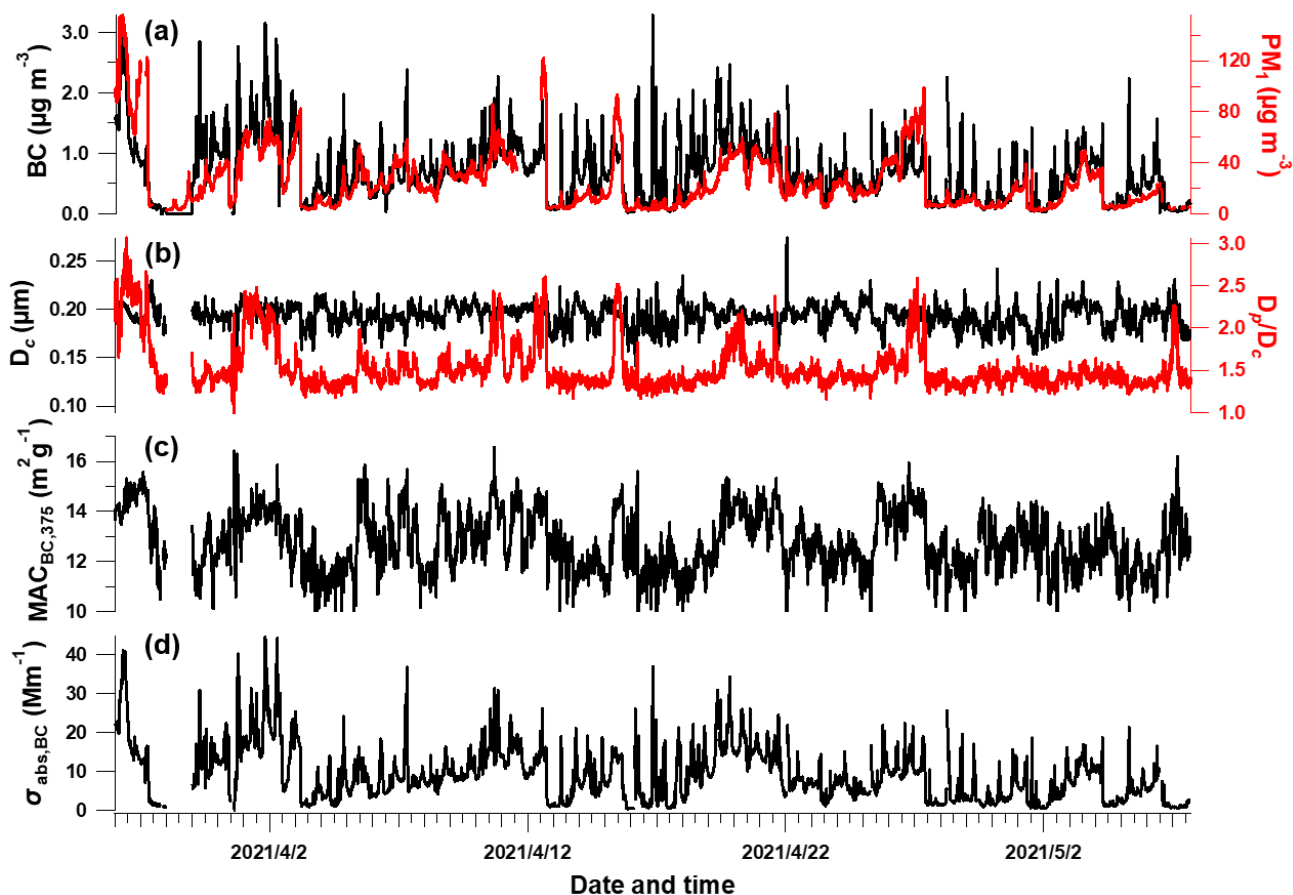


215
 216 **Figure 1. Information of source-apportioned organic aerosols by the PMF analysis. Mass spectra of (a) oxygenated OA1 (OOA1), (b)**
 217 **oxygenated OA2 (OOA2), (c) biomass burning OA (BBOA), (d) cooking-related OA (COA), (e) hydrocarbon-like OA (HOA), (f-j)**
 218 **Temporal variations of each PMF factor and the corresponding marker species. (k-o) Diurnal profiles of each factor. The lines, dots**
 219 **and whiskers denote the median, mean and the 25th/75th percentiles at each hour respectively.**

220 3.2 Segregated aerosol absorption

221 Fig. 2 shows the time series of BC properties, including the BC mass concentration, D_p/D_c , D_c , MAC and light absorption
 222 coefficient of BC (section 2.2). The MMD of BC core varied between 93 – 274 nm which may correspond to the source-
 223 specific information (Liu et al., 2019b) or coagulation process during ageing. The coating of BC (indicated by D_p/D_c) showed
 224 sporadic enhancement which was closely associated with enhanced PM concentration (Fig. 2a). This was consistent with
 225 previous studies that high coatings of BC occurred during heavier pollution due to the enhanced secondary formation of
 226 condensable materials to particle phase (Ding et al., 2019; Zhang et al., 2018). This clearly indicates the variation of mixing
 227 state of BC and this will potentially influence its MAC and absorption Ångström exponent (AAE) (Liu et al., 2015a). It will
 228 introduce considerable uncertainties to use constant MAC or AAE to derive the absorption coefficient of BC at multiple

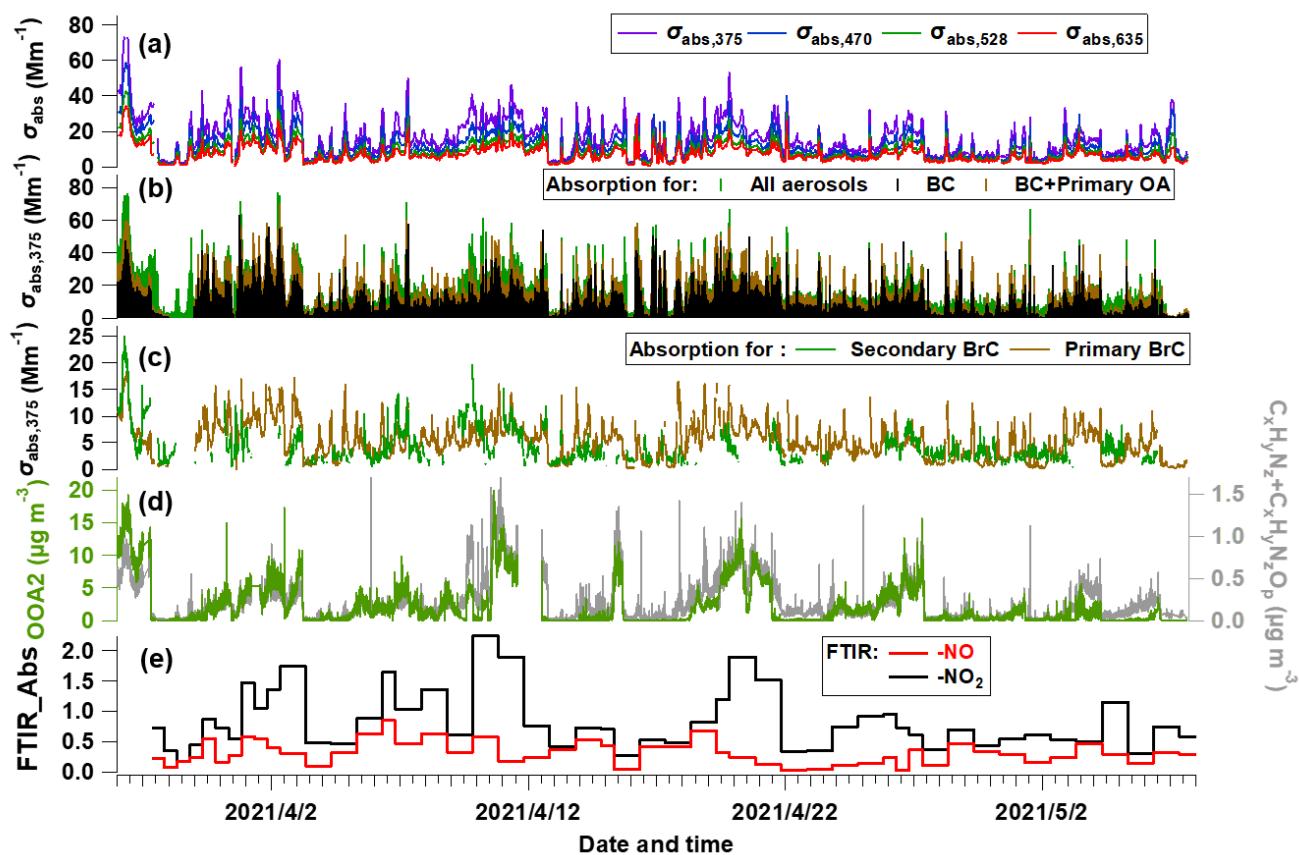
229 wavelengths. The MAC estimated using the measured BC core size and coatings (Fig. 2c) is thus used to derive the $\sigma_{\text{abs,BC}}$
 230 (section 2.2, shown in Fig. 2d). The $\sigma_{\text{abs,BC}}$ was $9.1 \pm 7.3 \text{ Mm}^{-1}$ during experimental period. MAC of BC at $\lambda=375\text{nm}$ showed to
 231 be at $8.4 - 16.6 \text{ m}^2 \text{ g}^{-1}$ with enhanced absorption when high coatings, which was consistent with previous studies which reported
 232 MAC_{BC} of $8-10 \text{ m}^2 \text{ g}^{-1}$, and higher value of $9.7 - 17.2 \text{ m}^2 \text{ g}^{-1}$ under polluted condition (Ding et al., 2019; Hu et al., 2021). The
 233 uncertainty of $\left(\frac{\sigma_{\text{abs,total}}}{[\text{rBC}]_{\text{pri}}}\right)$ is 4% for the data points over 1.5 according to (Wang et al., 2019a). The measurement of rBC
 234 mass from the SP2 had uncertainty of 20% (Schwarz et al., 2008), with relative coating thickness having uncertainty of 23%
 235 (Taylor et al., 2015), hereby resulting in a uncertainty of 27% for calculated MAC_{BC} . The above results in uncertainties of 31%
 236 and 20% for $\sigma_{\text{abs,BC}}$ and $\sigma_{\text{abs,pri}}$, respectively. The absorption measurement by MA200 had uncertainty of 25% (Drinovec et al.,
 237 2015b; Duesing et al., 2019). All these uncertainties propagates the uncertainties of $\sigma_{\text{abs,BrC}}$, $\sigma_{\text{abs,priBrC}}$ and $\sigma_{\text{abs,secBrC}}$ as 40%, 37%
 238 and 32% respectively. These are summarized in Table S1.



239
 240 **Figure 2. Temporal evolution of BC-related properties. (a) rBC and PM₁ mass concentration, (b) BC core diameter and bulk coating**
 241 **thickness (D_p/D_c), (c) calculated mass absorption cross section (MAC) at $\lambda=375\text{nm}$, (d) absorption coefficient of BC.**

242 Using the method above, the total ($\sigma_{\text{abs,total}}$) and attributed absorption of BC ($\sigma_{\text{abs,BC}}$), primary ($\sigma_{\text{abs,priBrC}}$) and secondary BrC

243 ($\sigma_{\text{abs,secBrC}}$) at $\lambda=375\text{nm}$ are shown in Fig. 3a-c. In Fig. 3b, the brown and green shades above the adjacent tracer indicate the
 244 absorption coefficient of primary and secondary BrC, respectively. Fig. 3c shows that the absorption coefficient of primary
 245 BrC was higher than secondary BrC for most time, but for certain periods they were equivalent or secondary BrC occasionally
 246 exceeds primary BrC. The mean contribution of absorption coefficient for BC, primary BrC and secondary BrC is 51%, 27%
 247 and 22% in this study. The tracers associated with nitrogen-containing organics, such as OOA2 (with highest N/C), $\text{C}_x\text{H}_y\text{N}_z$
 248 and $\text{C}_x\text{H}_y\text{N}_z\text{O}_p$ fragments, and the FTIR measured $-\text{NO} + -\text{NO}_2$, are also shown in Fig. 3d-e.



249
 250 **Figure 3. Temporal evolution of segregated absorbing properties.** (a) Absorbing coefficients (σ_{abs}) at multiple wavelengths measured
 251 by the aethalometer, (b) σ_{abs} at $\lambda=375\text{nm}$ ($\sigma_{\text{abs,375}}$) for all aerosols, primary OA and BC, (c) $\sigma_{\text{abs,375}}$ for primary BrC and secondary
 252 BrC. (d) mass concentration of OOA2 and the $\text{C}_x\text{H}_y\text{N}_z$ and $\text{C}_x\text{H}_y\text{N}_z\text{O}_p$ fragments measured by the AMS. (e) FTIR-measured
 253 absorption of $-\text{NO}$ and $-\text{NO}_2$ bonds.

254 3.3 Source attribution of BrC absorption

255 A multiple linear regression (MLR) analysis is performed to apportion the absorption coefficient of BrC with the PMF
 256 attributed OA factors, expressed as:

$$257 \sigma_{\text{abs,BrC}} = a_0 + a_1 \cdot [\text{OOA1}] + a_2 \cdot [\text{OOA2}] + a_3 \cdot [\text{BBOA}] + a_4 \cdot [\text{COA}] + a_5 \cdot [\text{HOA}] \quad (6)$$

258 where a_1 to a_5 represents the regression coefficients for each factor. These coefficients can be associated with the absorptivity

259 of each factor, i.e., a larger coefficient implies a higher MAC for the source associated with that OA factor (Kasthuriarachchi
 260 et al., 2020; Wang et al., 2021). The BBOA was found to have the highest MAC at $2.59 \text{ m}^2 \text{ g}^{-1}$, consistent with previous studies
 261 which also found significantly higher absorption for biomass burning source (Qin et al., 2018; Wang et al., 2019b; Zhang et
 262 al., 2022). The other POA factors generally have a higher MAC than SOA (the MAC of HOA and COA are $1.70 \text{ m}^2 \text{ g}^{-1}$ and
 263 $1.30 \text{ m}^2 \text{ g}^{-1}$, respectively). Particularly, the OOA2 has a relatively high MAC of $1.22 \text{ m}^2 \text{ g}^{-1}$, which is likely to result from the
 264 production of secondary BrC as discussed below. The contribution of each source-specific OA factor to $\sigma_{\text{abs,BrC}}$ can also be
 265 obtained. This analysis is performed for the total BrC, primary and secondary BrC respectively. The results are shown in Table
 266 1. MLR on the total BrC shows relatively higher correction ($r > 0.4$) with the factors of HOA, BBOA and OOA2, suggesting
 267 the potential importance of the primary biomass burning and traffic source along with OOA2 in governing absorption of BrC.
 268 MLR analysis on the primary BrC distinguishes its substantial correlation with BBOA ($r = 0.40$) and HOA ($r = 0.46$), while MLR
 269 on the secondary BrC has a high correlation with OOA2 only ($r = 0.44$). The MLR analysis links the apportioned absorption of
 270 physical properties with source-attributed chemical compositions, therefore validating and identifying the sources of primary
 271 and secondary BrC.

272 **Table 1. Results of the multilinear regression analysis (MLR) between $\sigma_{\text{abs,375}}$ and the five PMF-resolved OA factors, with $\sigma_{\text{abs,375}}$ of**
 273 **total BrC, primary and secondary BrC as dependent, respectively. All regression coefficients have passed the significance test with**
 274 **$p < 0.01$. Partial correlations above 0.4 are marked in bold. Since negative values appear when the COA participates, which is thus**
 275 **not included in the final regression but the values using COA factor are shown in brackets.**

Dependent	$\sigma_{\text{abs,BrC}}$		$\sigma_{\text{abs,pri BrC}}$		$\sigma_{\text{abs,sec BrC}}$	
	Regression coefficient	Partial correlation	Regression coefficient	Partial correlation	Regression coefficient	Partial correlation
Constant	2.26		1.67		1.47 (1.52)	
OOA1	0.57	0.23	0.04	0.02	0.46(0.46)	0.24 (0.24)
OOA2	1.22	0.53	0.37	0.25	0.74 (0.74)	0.44 (0.44)
BBOA	2.59	0.46	1.22	0.40	1.14 (1.18)	0.29 (0.29)
COA	1.30	0.22	1.45	0.36	/ (-0.25)	/ (-0.05)
HOA	1.70	0.47	1.17	0.46	0.49 (0.52)	0.20 (0.21)
R ²		0.77		0.63		0.55 (0.55)

276 Importantly, an oxygenated secondary OA factor (OOA2) is identified to significantly contribute to the secondary BrC. This
 277 OOA has a moderate O/C (0.62) and a highest N/C of 0.037 among all factors. The high N/C means this factor contains the
 278 most abundant nitrogen-containing fragments, implied as its high correlation with the $\text{C}_x\text{H}_y\text{N}_z$ and $\text{C}_x\text{H}_y\text{N}_z\text{O}_p$ fragments ($r = 0.83$,
 279 Fig. 3d) and with the FTIR absorption for $-\text{NO}_2$ and $-\text{NO}$ bonds ($r = 0.69$, Fig. S4). The $-\text{NO}$ bond is mostly related to the
 280 organic nitrates (RONO_2), and $-\text{NO}_2$ peak could result from both organic nitrates and nitro-organics (Bruns et al., 2010). There

281 is no discernable peak for organic amines. These all consistently imply that the OOA2 factor contained substantial fraction of
282 nitrogen-containing organics, and these compounds have contributed to the absorption of secondary BrC.

283 **3.4 Simultaneous whitening and darkening process of BrC**

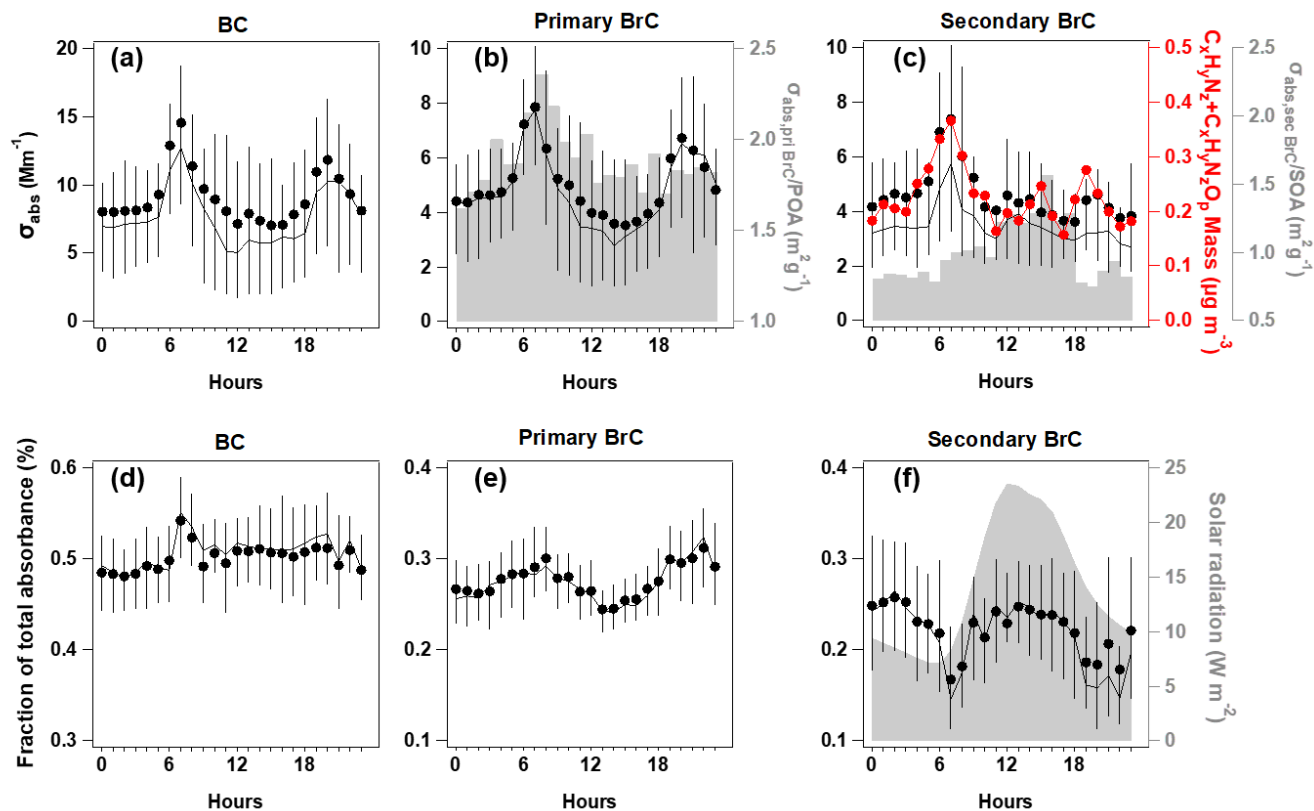
284 The relative contribution and diurnal variation of primary and secondary BrC measured by MA200 at 470, 528 and 635nm
285 wavelengths are similar to those at 375nm wavelengths, but with decreased fraction of BrC absorption with increased
286 wavelength. The mean AAE of total BrC, primary BrC and secondary BrC is obtained by power fitting on the mean absorption
287 coefficient during the experiment (Fig.S7), which is 6.16, 5.69 and 6.40 respectively. This is consistent with other studies that
288 SOA usually had a higher AAE than POA (Gilardoni et al., 2016; Jiang et al., 2022). Due to the high contribution of BC to total
289 absorption (>50% even at shortest wavelength), the spectral dependence of absorption in bulk has not shown apparent diurnal
290 variation. The diurnal variation of $\sigma_{\text{abs},375}$ for BC and primary BrC and their fractions showed consistent morning rush-hour
291 peaks at 6:00-8:00 and the night-time enhancement due to reduced boundary layer (Fig. 4a-b). This was in line with the morning
292 peak of HOA and night peak of BBOA. The traffic source in this region, in particular the diesel vehicles, was reported to emit
293 considerable OA with certain chromophores, such as aromatics (Yao et al., 2015) and heterocyclic organic compounds (Gentner
294 et al., 2017; Schuetzle, 1983). In the morning rush-hour, BC and primary BrC accounted for $51\pm4\%$ and $29\pm4\%$ in the total
295 $\sigma_{\text{abs},375}$ respectively, with the remaining $20\pm2\%$ classified as secondary BrC. The morning peak coinciding with the primary
296 BrC may result from the rapid formation of BrC from sources when emitted gases condensed and formed aerosols. These may
297 lead to high cooccurrence between primary and secondary BrC. Previous studies in urban environment also observed
298 concurrent peaks of primary and secondary BrC, which usually occurred at morning rush hour (Zhang et al., 2020).
299 Furthermore, the assumption of the method used to apportion primary and secondary BrC will cause some error in the
300 distinction of absorption coefficient, it is possible that some of the primary sources are being attributed to secondary sources
301 and vice versa. This maybe a possible reason for the simultaneous peak observed for primary and secondary BrC during
302 morning rush hour. The night had contributions from BC and primary BrC at $50\pm2\%$ and $30\pm3\%$ respectively, with $20\pm3\%$ as
303 secondary BrC. Fig. 4b showed the decrease of primary BrC absorption tended to be more rapid than the HOA and BBOA
304 mass (even a slight increase for HOA Fig. 1m and Fig. 1o) in the midday, leading to decreased absorption coefficient per unit
305 mass of primary BrC (shade in Fig. 4b), which indicates the decrease of BrC absorptivity likely due to photochemistry. This
306 may involve the OH radical reaction with existing chromophores in aerosol phase (Schnitzler et al., 2020) or by enhanced
307 evaporation of aerosols to gas phase (Palm et al., 2020) leading to further decrease of BrC absorptivity during midday. In
308 addition to photobleaching, it possible that some primary species transformed into less absorbing secondary BrC species.
309 During this period, the type of HOA or BBOA that contribute to absorption may also have a lower absorptivity. In this context,
310 a recent chamber study reported that the primary BrC from biomass burning plumes could be bleached to half of the initial
311 absorptivity in 2-3 hours (Liu et al., 2021). The reaction of BrC with OH radical has been widely recognized as the main
312 pathway for the loss of primary BrC absorptivity (Liu et al., 2020), and was parameterized as an exponential decrease with

313 time at certain OH radical concentration in global scale (Wang et al., 2018b).

314 Besides the morning rush-hour peak, there was an early afternoon peak for the absorption coefficient of secondary BrC,
315 prevailing the dilution effect of daytime boundary layer (Fig. 4c-S5). The night and morning peak of OOA2 and the morning
316 peak of $\sigma_{\text{abs,secBrC}}$ may result from primarily emitted moderately oxygenated OA, which was reported from some diesel sources
317 (Dewitt et al., 2015; Gentner et al., 2012). The fraction of secondary BrC thus had a pronounced early afternoon peak soon
318 after the peak solar radiation (Fig. 4f) and a peak after midnight soon after the nighttime peak of primary BrC (Fig. 4e). Fig.
319 4b showed that the MAC of POA decreased after the morning peak. The MAC of SOA showed an afternoon peak (Fig. 4c),
320 indicating the enhancement of absorption efficiency of secondary BrC, which occurred in a few hours after the peak solar
321 radiation. This means the photochemistry caused the absorptivity of POA decreased but the absorptivity of SOA increased. Fig
322 4e-f shows the photochemical processes led to an enhanced contribution of secondary BrC to the total absorption by 30% from
323 the morning rush-hour to midday, but during the same time reduced the contribution of primary BrC to the total absorption
324 about 20%. Though the other process such as aqueous reactions at nighttime may also contribute the change of MAC for BrC,
325 the apparent change in the daytime was indeed observed in this study, and the absorption of aerosols plays a more important
326 role on the radiative impacts in the daytime when intensive solar radiation. This shift of peaking time from primary to secondary
327 BrC demonstrates the likely process of SOA formation from gases, and these SOA compounds containing nitrogen (i.e., the
328 OOA2) considerably contributed to the light absorption. This ageing or oxidation likely occurred through photooxidation
329 during early afternoon and aqueous processes (high RH conditions prevail during nighttime) during nighttime. The oxidized
330 volatile organic compounds (VOCs) with nitrogen chemistry involved could condense to produce additional mass in particle
331 phase (Ehn et al., 2014; Finewax et al., 2018). Due to the high NO_x emission, photooxidation of traffic VOCs may have largely
332 involved nitrogen chemistry. Previous studies found the NO_x -involved SOA could produce considerable chromophores (Lin et
333 al., 2015; Siemens et al., 2022), such as the traffic VOCs may produce SOA in a time scale of hours, containing nitro-aromatics
334 (Wang et al., 2019d; Keyte et al., 2016). The daytime formation of organic nitrate may follow the gas-phase photooxidation
335 mechanism, in which the excess NO could add to the peroxy radical to produce organic nitrate (Liebmann et al., 2019). The
336 nighttime chemistry involving NO_3 radical through the oxidation of NO_2 by O_3 , contributed to the important formation of
337 organic nitrate by initializing the production of nitrooxy peroxy radicals (Ng et al., 2008; Rollins et al., 2012). Laboratory
338 studies (Nakayama et al., 2013; Liu et al., 2015c) also widely observed the rapid production of nitrogen-containing OA
339 involving NO_x chemistry could contribute to light absorption of aerosols.

340 Overall, by apportioning the absorption of primary and secondary BrC, the BBOA was found to have the highest MAC and
341 the other POA factors generally have a higher MAC than SOA, the OOA2 has a relatively high MAC which is likely to result
342 from the production of secondary BrC. We found the photochemical processes decreased the MAC of POA but increased the
343 MAC of SOA, resulting in an enhanced contribution of secondary BrC to total absorbance by 30% but reduced contribution
344 of primary BrC about 20% in the semi-urban environment. This revealed that the whitening and darkening of BrC occurred
345 simultaneously, and the secondary BrC produced by photooxidation may compensate some bleaching effect of primary BrC.
346 The dominance of both competing processes may depend on the timescale and altitude in the atmosphere. For example, the

347 enhanced BrC fraction observed above the planetary boundary layer may be explained by the enhanced secondary BrC (Tian
 348 et al., 2020), while further ageing may bleach the produced chromophores of these SOA.



349
 350 **Figure 4. Diurnal variations of absorption coefficient at $\lambda=375\text{nm}$ ($\sigma_{\text{abs},375}$) for BC (a), primary BrC and absorption efficiency of**
 351 **primary BrC ($\sigma_{\text{abs,pri BrC}}/\text{POA}$) is shown in shade (b), secondary BrC and absorption efficiency of secondary BrC ($\sigma_{\text{abs,sec BrC}}/\text{SOA}$) is**
 352 **shown in shade, along with the $\text{C}_x\text{H}_y\text{N}_z$ and $\text{C}_x\text{H}_y\text{N}_z\text{O}_p$ fragments (c); the respective fraction in total for the segregated $\sigma_{\text{abs},375}$ (d-f),**
 353 **with direct radiation shown in shade. In each plot, the lines, dots and whiskers denote the median, mean and the 25th/75th percentiles**
 354 **at each hour respectively.**

355 4. Conclusion

356 This study apportioned the shortwave absorption of BC, primary and secondary BrC, through concurrent measurements of BC
 357 microphysical properties and OA mass spectra. The apportioned primary BrC absorption was linked with traffic and biomass
 358 burning emissions, while secondary BrC was found to be associated with an oxygenated secondary OA factor with higher
 359 nitrogen content. The enhancement of secondary BrC and decrease of primary BrC simultaneously occurred via daytime
 360 photooxidation. The results emphasize the importance of nitrogen-containing OA in contributing to BrC. These OA could
 361 primarily emit as aerosol phase, or in gas phase which requires further oxidation to be in aerosol phase to serve as BrC. The
 362 NO_x -involved chemistry is prone to add nitrogen element to the existing OA and enhance the absorptivity of chromophores.
 363 The anthropogenic NO_x emission could be therefore an important source in producing shortwave absorbing components in the

364 atmosphere, which may offset some of the conventionally-thought photobleaching of BrC by photochemistry. The production
365 of secondary BrC should be considered when assessing the environment and climate impacts of light-absorbing aerosols.

366 **Acknowledgments**

367 This research was supported by the National Natural Science Foundation of China (Grant No. 42175116 and 41875167),
368 National Key R&D Program of China (2019YFC0214703).

369 **Author contribution**

370 D.L., X.J. and Qian L. prepared and designed the observation. D.L., Qian L., X.J and P.T. initiated the field campaign and
371 conducted the measurements. Qian L., D.L. P.T., Y.W., S.L. and K.H. contributed to the data analysis. Qian L., H.M., L.R.,
372 B.K., D.D. and S.K. provided technical support and assistance. Qian L. and D.L. wrote the manuscript. All authors read and
373 approved the final manuscript.

374

375 **References**

- 376 Aiken, A. C., Salcedo, D., Cubison, M. J., Huffman, J. A., DeCarlo, P. F., Ulbrich, I. M., Docherty, K. S., Sueper, D., Kimmel,
377 J. R., Worsnop, D. R., Trimborn, A., Northway, M., Stone, E. A., Schauer, J. J., Volkamer, R. M., Fortner, E., de Foy, B., Wang,
378 J., Laskin, A., Shutthanandan, V., Zheng, J., Zhang, R., Gaffney, J., Marley, N. A., Paredes-Miranda, G., Arnott, W. P., Molina,
379 L. T., Sosa, G., and Jimenez, J. L.: Mexico City aerosol analysis during MILAGRO using high resolution aerosol mass
380 spectrometry at the urban supersite (T0) - Part 1: Fine particle composition and organic source apportionment, *Atmos Chem*
381 *Phys*, 9, 6633-6653, doi:10.5194/acp-9-6633-2009, 2009.
- 382 Andreae, M. O. and Crutzen, P. J.: Atmospheric aerosols: Biogeochemical sources and role in atmospheric chemistry, *Science*,
383 276, 1052-1058, doi:10.1126/science.276.5315.1052, 1997.
- 384 Bahadur, R., Praveen, P. S., Xu, Y., and Ramanathan, V.: Solar absorption by elemental and brown carbon determined from
385 spectral observations, *Proceedings of the National Academy of Sciences of the United States of America*, 109, 17366-17371,
386 doi:10.1073/pnas.1205910109, 2012.
- 387 Bond, T. C.: Spectral dependence of visible light absorption by carbonaceous particles emitted from coal combustion,
388 *Geophysical Research Letters*, 28, 4075-4078, doi:10.1029/2001gl013652, 2001.
- 389 Bond, T. C. and Bergstrom, R. W.: Light absorption by carbonaceous particles: An investigative review, *Aerosol Science and*
390 *Technology*, 40, 27-67, doi:10.1080/02786820500421521, 2006.
- 391 Brown, S. G., Lee, T., Roberts, P. T., and Collett, J. L., Jr.: Wintertime Residential Biomass Burning in Las Vegas, Nevada;
392 Marker Components and Apportionment Methods, *Atmosphere*, 7, doi:10.3390/atmos7040058, 2016.
- 393 Bruns, E. A., Perraud, V., Zelenyuk, A., Ezell, M. J., Johnson, S. N., Yu, Y., Imre, D., Finlayson-Pitts, B. J., and Alexander, M.
394 L.: Comparison of FTIR and Particle Mass Spectrometry for the Measurement of Particulate Organic Nitrates, *Environmental*
395 *Science & Technology*, 44, 1056-1061, 10.1021/es9029864, 2010.
- 396 Canagaratna, M. R., Jimenez, J. L., Kroll, J. H., Chen, Q., Kessler, S. H., Massoli, P., Hildebrandt Ruiz, L., Fortner, E., Williams,
397 L. R., Wilson, K. R., Surratt, J. D., Donahue, N. M., Jayne, J. T., and Worsnop, D. R.: Elemental ratio measurements of organic
398 compounds using aerosol mass spectrometry: characterization, improved calibration, and implications, *Atmospheric Chemistry*
399 *and Physics*, 15, 253-272, doi:10.5194/acp-15-253-2015, 2015.
- 400 Canagaratna, M. R., Jayne, J. T., Jimenez, J. L., Allan, J. D., Alfarra, M. R., Zhang, Q., Onasch, T. B., Drewnick, F., Coe, H.,
401 Middlebrook, A., Delia, A., Williams, L. R., Trimborn, A. M., Northway, M. J., DeCarlo, P. F., Kolb, C. E., Davidovits, P., and
402 Worsnop, D. R.: Chemical and microphysical characterization of ambient aerosols with the aerodyne aerosol mass spectrometer,
403 *Mass Spectrometry Reviews*, 26, 185-222, doi:10.1002/mas.20115, 2007.
- 404 Cheng, Y., Engling, G., He, K. B., Duan, F. K., Ma, Y. L., Du, Z. Y., Liu, J. M., Zheng, M., and Weber, R. J.: Biomass burning
405 contribution to Beijing aerosol, *Atmospheric Chemistry and Physics*, 13, 7765-7781, doi:10.5194/acp-13-7765-2013, 2013.
- 406 Coury, C. and Dillner, A. M.: A method to quantify organic functional groups and inorganic compounds in ambient aerosols
407 using attenuated total reflectance FTIR spectroscopy and multivariate chemometric techniques, *Atmospheric Environment*, 42,

408 5923-5932, doi:10.1016/j.atmosenv.2008.03.026, 2008.

409 Crilley, L. R., Bloss, W. J., Yin, J., Beddows, D. C. S., Harrison, R. M., Allan, J. D., Young, D. E., Flynn, M., Williams, P.,
410 Zotter, P., Prevot, A. S. H., Heal, M. R., Barlow, J. F., Halios, C. H., Lee, J. D., Szidat, S., and Mohr, C.: Sources and
411 contributions of wood smoke during winter in London: assessing local and regional influences, *Atmos Chem Phys*, 15, 3149-
412 3171, doi:10.5194/acp-15-3149-2015, 2015.

413 Cubison, M. J., Ortega, A. M., Hayes, P. L., Farmer, D. K., Day, D., Lechner, M. J., Brune, W. H., Apel, E., Diskin, G. S.,
414 Fisher, J. A., Fuelberg, H. E., Hecobian, A., Knapp, D. J., Mikoviny, T., Riemer, D., Sachse, G. W., Sessions, W., Weber, R. J.,
415 Weinheimer, A. J., Wisthaler, A., and Jimenez, J. L.: Effects of aging on organic aerosol from open biomass burning smoke in
416 aircraft and laboratory studies, *Atmos Chem Phys*, 11, 12049-12064, doi:10.5194/acp-11-12049-2011, 2011.

417 Dasari, S., Andersson, A., Bikkina, S., Holmstrand, H., Budhavant, K., Satheesh, S., Asmi, E., Kesti, J., Backman, J., Salam,
418 A., Bisht, D. S., Tiwari, S., Hameed, Z., and Gustafsson, O.: Photochemical degradation affects the light absorption of water-
419 soluble brown carbon in the South Asian outflow, *Science Advances*, 5, doi:10.1126/sciadv.aau8066, 2019.

420 DeCarlo, P. F., Ulbrich, I. M., Crouse, J., de Foy, B., Dunlea, E. J., Aiken, A. C., Knapp, D., Weinheimer, A. J., Campos, T.,
421 Wennberg, P. O., and Jimenez, J. L.: Investigation of the sources and processing of organic aerosol over the Central Mexican
422 Plateau from aircraft measurements during MILAGRO, *Atmospheric Chemistry and Physics*, 10, 5257-5280, doi:10.5194/acp-
423 10-5257-2010, 2010.

424 DeWitt, H. L., Hellebust, S., Temime-Roussel, B., Ravier, S., Polo, L., Jacob, V., Buisson, C., Charron, A., Andre, M., Pasquier,
425 A., Besombes, J. L., Jaffrezo, J. L., Wortham, H., and Marchand, N.: Near-highway aerosol and gas-phase measurements in a
426 high-diesel environment, *Atmospheric Chemistry and Physics*, 15, 4373-4387, doi:10.5194/acp-15-4373-2015, 2015.

427 Ding, S., Liu, D., Zhao, D., Hu, K., Tian, P., Zhou, W., Huang, M., Yang, Y., Wang, F., Sheng, J., Liu, Q., Kong, S., Cui, P.,
428 Huang, Y., He, H., Coe, H., and Ding, D.: Size-Related Physical Properties of Black Carbon in the Lower Atmosphere over
429 Beijing and Europe, *Environmental Science & Technology*, 53, 11112-11121, doi:10.1021/acs.est.9b03722, 2019.

430 Draxier, R. R. and Hess, G. D.: An overview of the HYSPLIT_4 modelling system for trajectories, dispersion and deposition,
431 *Australian Meteorological Magazine*, 47, 295-308, 1998.

432 Drinovec, L., Mo?Nik, G., Zotter, P., Prév?t, A. S. H., Ruckstuhl, C., Coz, E., Rupakheti, M., Sciare, J., Müller, T., and
433 Wiedensohler, A.: The "dual-spot" Aethalometer: an improved measurement of aerosol black carbon with real-time loading
434 compensation, *Atmospheric Measurement Techniques*, 8, 1965-1979, 2015a.

435 Drinovec, L., Močnik, G., Zotter, P., Prévôt, A. S. H., Ruckstuhl, C., Coz, E., Rupakheti, M., Sciare, J., Müller, T., Wiedensohler,
436 A., and Hansen, A. D. A.: The "dual-spot" Aethalometer: an improved measurement of aerosol black carbon with real-time
437 loading compensation, *Atmos. Meas. Tech.*, 8, 1965-1979, doi:10.5194/amt-8-1965-2015, 2015b.

438 Duesing, S., Wehner, B., Mueller, T., Stoecker, A., and Wiedensohler, A.: The effect of rapid relative humidity changes on fast
439 filter-based aerosol-particle light-absorption measurements: uncertainties and correction schemes, *Atmospheric Measurement*
440 *Techniques*, 12, 5879-5895, doi:10.5194/amt-12-5879-2019, 2019.

441 Ehn, M., Thornton, J. A., Kleist, E., Sipila, M., Junninen, H., Pullinen, I., Springer, M., Rubach, F., Tillmann, R., Lee, B.,

442 Lopez-Hilfiker, F., Andres, S., Acir, I.-H., Rissanen, M., Jokinen, T., Schobesberger, S., Kangasluoma, J., Kontkanen, J.,
443 Nieminen, T., Kurten, T., Nielsen, L. B., Jorgensen, S., Kjaergaard, H. G., Canagaratna, M., Dal Maso, M., Berndt, T., Petaja,
444 T., Wahner, A., Kerminen, V.-M., Kulmala, M., Worsnop, D. R., Wildt, J., and Mentel, T. F.: A large source of low-volatility
445 secondary organic aerosol, *Nature*, 506, 476-+, doi:10.1038/nature13032, 2014.

446 Elser, M., Huang, R.-J., Wolf, R., Slowik, J. G., Wang, Q., Canonaco, F., Li, G., Bozzetti, C., Daellenbach, K. R., Huang, Y.,
447 Zhang, R., Li, Z., Cao, J., Baltensperger, U., El-Haddad, I., and Prevot, A. S. H.: New insights into PM_{2.5} chemical
448 composition and sources in two major cities in China during extreme haze events using aerosol mass spectrometry, *Atmos*
449 *Chem Phys*, 16, 3207-3225, doi:10.5194/acp-16-3207-2016, 2016.

450 Finewax, Z., de Gouw, J. A., and Ziemann, P. J.: Identification and Quantification of 4-Nitrocatechol Formed from OH and
451 NO₃ Radical-Initiated Reactions of Catechol in Air in the Presence of NO_x: Implications for Secondary Organic Aerosol
452 Formation from Biomass Burning, *Environmental Science & Technology*, 52, 1981-1989, doi:10.1021/acs.est.7b05864, 2018.

453 Forrister, H., Liu, J., Scheuer, E., Dibb, J., Ziemba, L., Thornhill, K. L., Anderson, B., Diskin, G., Perring, A. E., Schwarz, J.
454 P., Campuzano-Jost, P., Day, D. A., Palm, B. B., Jimenez, J. L., Nenes, A., and Weber, R. J.: Evolution of brown carbon in
455 wildfire plumes, *Geophysical Research Letters*, 42, 4623-4630, doi:10.1002/2015gl063897, 2015.

456 Gao, Y., Wang, Q., Li, L., Dai, W., Yu, J., Ding, L., Li, J., Xin, B., Ran, W., Han, Y., and Cao, J.: Optical properties of mountain
457 primary and secondary brown carbon aerosols in summertime, *Science of the Total Environment*, 806,
458 10.1016/j.scitotenv.2021.150570, 2022.

459 Gentner, D. R., Isaacman, G., Worton, D. R., Chan, A. W. H., Dallmann, T. R., Davis, L., Liu, S., Day, D. A., Russell, L. M.,
460 Wilson, K. R., Weber, R., Guha, A., Harley, R. A., and Goldstein, A. H.: Elucidating secondary organic aerosol from diesel and
461 gasoline vehicles through detailed characterization of organic carbon emissions, *Proceedings of the National Academy of*
462 *Sciences of the United States of America*, 109, 18318-18323, doi:10.1073/pnas.1212272109, 2012.

463 Gentner, D. R., Jathar, S. H., Gordon, T. D., Bahreini, R., Day, D. A., El Haddad, I., Hayes, P. L., Pieber, S. M., Platt, S. M.,
464 de Gouw, J., Goldstein, A. H., Harley, R. A., Jimenez, J. L., Prevot, A. S. H., and Robinson, A. L.: Review of Urban Secondary
465 Organic Aerosol Formation from Gasoline and Diesel Motor Vehicle Emissions, *Environmental Science & Technology*, 51,
466 1074-1093, doi:10.1021/acs.est.6b04509, 2017.

467 Gilardoni, S., Massoli, P., Paglione, M., Giulianelli, L., Carbone, C., Rinaldi, M., Decesari, S., Sandrini, S., Costabile, F.,
468 Gobbi, G. P., Pietrogrande, M. C., Visentin, M., Scotto, F., Fuzzi, S., and Facchini, M. C.: Direct observation of aqueous
469 secondary organic aerosol from biomass-burning emissions, *Proceedings of the National Academy of Sciences of the United*
470 *States of America*, 113, 10013-10018, 10.1073/pnas.1602212113, 2016.

471 Hayes, P. L., Ortega, A. M., Cubison, M. J., Froyd, K. D., Zhao, Y., Cliff, S. S., Hu, W. W., Toohey, D. W., Flynn, J. H., Lefer,
472 B. L., Grossberg, N., Alvarez, S., Rappenglueck, B., Taylor, J. W., Allan, J. D., Holloway, J. S., Gilman, J. B., Kuster, W. C.,
473 De Gouw, J. A., Massoli, P., Zhang, X., Liu, J., Weber, R. J., Corrigan, A. L., Russell, L. M., Isaacman, G., Worton, D. R.,
474 Kreisberg, N. M., Goldstein, A. H., Thalman, R., Waxman, E. M., Volkamer, R., Lin, Y. H., Surratt, J. D., Kleindienst, T. E.,
475 Offenberg, J. H., Dusanter, S., Griffith, S., Stevens, P. S., Brioude, J., Angevine, W. M., and Jimenez, J. L.: Organic aerosol

476 composition and sources in Pasadena, California, during the 2010 CalNex campaign, *Journal of Geophysical Research-*
477 *Atmospheres*, 118, 9233-9257, doi:10.1002/jgrd.50530, 2013.

478 Hu, K., Liu, D., Tian, P., Wu, Y., Deng, Z., Wu, Y., Zhao, D., Li, R., Sheng, J., Huang, M., Ding, D., Li, W., Wang, Y., and Wu,
479 Y.: Measurements of the Diversity of Shape and Mixing State for Ambient Black Carbon Particles, *Geophysical Research*
480 *Letters*, 48, doi:10.1029/2021gl094522, 2021.

481 Hu, W., Hu, M., Hu, W.-W., Zheng, J., Chen, C., Wu, Y., and Guo, S.: Seasonal variations in high time-resolved chemical
482 compositions, sources, and evolution of atmospheric submicron aerosols in the megacity Beijing, *Atmos Chem Phys*, 17, 9979-
483 10000, doi:10.5194/acp-17-9979-2017, 2017.

484 Huang, D. D., Zhu, S., An, J., Wang, Q., Qiao, L., Zhou, M., He, X., Ma, Y., Sun, Y., Huang, C., Yu, J. Z., and Zhang, Q.:
485 Comparative Assessment of Cooking Emission Contributions to Urban Organic Aerosol Using Online Molecular Tracers and
486 Aerosol Mass Spectrometry Measurements, *Environmental Science & Technology*, 55, 14526-14535,
487 doi:10.1021/acs.est.1c03280, 2021.

488 Huffman, J. A., Docherty, K. S., Aiken, A. C., Cubison, M. J., Ulbrich, I. M., DeCarlo, P. F., Sueper, D., Jayne, J. T., Worsnop,
489 D. R., Ziemann, P. J., and Jimenez, J. L.: Chemically-resolved aerosol volatility measurements from two megacity field studies,
490 *Atmospheric Chemistry and Physics*, 9, 7161-7182, doi:10.5194/acp-9-7161-2009, 2009.

491 Jacobson, M. Z.: Isolating nitrated and aromatic aerosols and nitrated aromatic gases as sources of ultraviolet light absorption,
492 *Journal of Geophysical Research-Atmospheres*, 104, 3527-3542, doi:10.1029/1998jd100054, 1999.

493 Jayne, J. T., Leard, D. C., Zhang, X. F., Davidovits, P., Smith, K. A., Kolb, C. E., and Worsnop, D. R.: Development of an
494 aerosol mass spectrometer for size and composition analysis of submicron particles, *Aerosol Science and Technology*, 33, 49-
495 70, doi:10.1080/027868200410840, 2000.

496 Jiang, X., Liu, D., Li, Q., Tian, P., Wu, Y., Li, S., Hu, K., Ding, S., Bi, K., Li, R., Huang, M., Ding, D., Chen, Q., Kong, S., Li,
497 W., Pang, Y., and He, D.: Connecting the Light Absorption of Atmospheric Organic Aerosols with Oxidation State and Polarity,
498 *Environmental science & technology*, doi:10.1021/acs.est.2c02202, 2022.

499 Jimenez, J. L., Canagaratna, M. R., Donahue, N. M., Prevot, A. S. H., Zhang, Q., Kroll, J. H., DeCarlo, P. F., Allan, J. D., Coe,
500 H., Ng, N. L., Aiken, A. C., Docherty, K. S., Ulbrich, I. M., Grieshop, A. P., Robinson, A. L., Duplissy, J., Smith, J. D., Wilson,
501 K. R., Lanz, V. A., Hueglin, C., Sun, Y. L., Tian, J., Laaksonen, A., Raatikainen, T., Rautiainen, J., Vaattovaara, P., Ehn, M.,
502 Kulmala, M., Tomlinson, J. M., Collins, D. R., Cubison, M. J., Dunlea, E. J., Huffman, J. A., Onasch, T. B., Alfarra, M. R.,
503 Williams, P. I., Bower, K., Kondo, Y., Schneider, J., Drewnick, F., Borrmann, S., Weimer, S., Demerjian, K., Salcedo, D.,
504 Cottrell, L., Griffin, R., Takami, A., Miyoshi, T., Hatakeyama, S., Shimono, A., Sun, J. Y., Zhang, Y. M., Dzepina, K., Kimmel,
505 J. R., Sueper, D., Jayne, J. T., Herndon, S. C., Trimborn, A. M., Williams, L. R., Wood, E. C., Middlebrook, A. M., Kolb, C.
506 E., Baltensperger, U., and Worsnop, D. R.: Evolution of Organic Aerosols in the Atmosphere, *Science*, 326, 1525-1529,
507 doi:10.1126/science.1180353, 2009.

508 Kasthuriarachchi, N. Y., Rivellini, L.-H., Adam, M. G., and Lee, A. K. Y.: Light Absorbing Properties of Primary and Secondary
509 Brown Carbon in a Tropical Urban Environment, *Environmental Science & Technology*, 54, 10808-10819,

510 10.1021/acs.est.0c02414, 2020.

511 Keyte, I. J., Albinet, A., and Harrison, R. M.: On-road traffic emissions of polycyclic aromatic hydrocarbons and their oxy-
512 and nitro-derivative compounds measured in road tunnel environments, *Science of the Total Environment*, 566, 1131-1142,
513 doi:10.1016/j.scitotenv.2016.05.152, 2016.

514 Laborde, M., Schnaiter, M., Linke, C., Saathoff, H., Naumann, K. H., Moehler, O., Berlenz, S., Wagner, U., Taylor, J. W., Liu,
515 D., Flynn, M., Allan, J. D., Coe, H., Heimerl, K., Dahlkoetter, F., Weinzierl, B., Wollny, A. G., Zanutta, M., Cozic, J., Laj, P.,
516 Hitzenberger, R., Schwarz, J. P., and Gysel, M.: Single Particle Soot Photometer intercomparison at the AIDA chamber,
517 *Atmospheric Measurement Techniques*, 5, 3077-3097, doi:10.5194/amt-5-3077-2012, 2012.

518 Laskin, A., Laskin, J., and Nizkorodov, S. A.: Chemistry of Atmospheric Brown Carbon, *Chemical Reviews*, 115, 4335-4382,
519 doi:10.1021/cr5006167, 2015.

520 Liebmann, J., Sobanski, N., Schuladen, J., Karu, E., Hellen, H., Hakola, H., Zha, Q., Ehn, M., Riva, M., Heikkinen, L.,
521 Williams, J., Fischer, H., Lelieveld, J., and Crowley, J. N.: Alkyl nitrates in the boreal forest: formation via the NO₃-, OH- and
522 O-3-induced oxidation of biogenic volatile organic compounds and ambient lifetimes, *Atmospheric Chemistry and Physics*,
523 19, 10391-10403, doi:10.5194/acp-19-10391-2019, 2019.

524 Lin, P., Liu, J., Shilling, J. E., Kathmann, S. M., Laskin, J., and Laskin, A.: Molecular characterization of brown carbon (BrC)
525 chromophores in secondary organic aerosol generated from photo-oxidation of toluene, *Physical Chemistry Chemical Physics*,
526 17, 23312-23325, doi:10.1039/c5cp02563j, 2015.

527 Liu, D., He, C., Schwarz, J. P., and Wang, X.: Lifecycle of light-absorbing carbonaceous aerosols in the atmosphere, *npj*
528 *Climate and Atmospheric Science*, 3, 40, doi:10.1038/s41612-020-00145-8, 2020.

529 Liu, D., Taylor, J. W., Young, D. E., Flynn, M. J., Coe, H., and Allan, J. D.: The effect of complex black carbon microphysics
530 on the determination of the optical properties of brown carbon, *Geophysical Research Letters*, 42, 613-619,
531 doi:10.1002/2014gl062443, 2015a.

532 Liu, D., Allan, J. D., Young, D. E., Coe, H., Beddows, D., Fleming, Z. L., Flynn, M. J., Gallagher, M. W., Harrison, R. M., Lee,
533 J., Prevot, A. S. H., Taylor, J. W., Yin, J., Williams, P. I., and Zotter, P.: Size distribution, mixing state and source apportionment
534 of black carbon aerosol in London during wintertime, *Atmos Chem Phys*, 14, 10061-10084, doi:10.5194/acp-14-10061-2014,
535 2014.

536 Liu, D., Joshi, R., Wang, J., Yu, C., Allan, J. D., Coe, H., Flynn, M. J., Xie, C., Lee, J., Squires, F., Kotthaus, S., Grimmond,
537 S., Ge, X., Sun, Y., and Fu, P.: Contrasting physical properties of black carbon in urban Beijing between winter and summer,
538 *Atmospheric Chemistry and Physics*, 19, 6749-6769, doi:10.5194/acp-19-6749-2019, 2019a.

539 Liu, D., Joshi, R., Wang, J., Yu, C., Allan, J. D., Coe, H., Flynn, M. J., Xie, C., Lee, J., Squires, F., Kotthaus, S., Grimmond,
540 S., Ge, X., Sun, Y., and Fu, P.: Contrasting physical properties of black carbon in urban Beijing between winter and summer,
541 *Atmos. Chem. Phys.*, 19, 6749-6769, doi:10.5194/acp-19-6749-2019, 2019b.

542 Liu, D., Li, S., Hu, D., Kong, S., Cheng, Y., Wu, Y., Ding, S., Hu, K., Zheng, S., Yan, Q., Zheng, H., Zhao, D., Tian, P., Ye, J.,
543 Huang, M., and Ding, D.: Evolution of Aerosol Optical Properties from Wood Smoke in Real Atmosphere Influenced by

544 Burning Phase and Solar Radiation, *Environmental Science & Technology*, 55, 5677-5688, doi:10.1021/acs.est.0c07569, 2021.

545 Liu, F., Zhang, Q., Tong, D., Zheng, B., Li, M., Huo, H., and He, K. B.: High-resolution inventory of technologies, activities,
546 and emissions of coal-fired power plants in China from 1990 to 2010, *Atmospheric Chemistry and Physics*, 15, 13299-13317,
547 doi:10.5194/acp-15-13299-2015, 2015b.

548 Liu, J., Mauzerall, D. L., Chen, Q., Zhang, Q., Song, Y., Peng, W., Klimont, Z., Qiu, X., Zhang, S., Hu, M., Lin, W., Smith, K.
549 R., and Zhu, T.: Air pollutant emissions from Chinese households: A major and underappreciated ambient pollution source,
550 *Proceedings of the National Academy of Sciences of the United States of America*, 113, 7756-7761,
551 doi:10.1073/pnas.1604537113, 2016.

552 Liu, P. F., Abdelmalki, N., Hung, H. M., Wang, Y., Brune, W. H., and Martin, S. T.: Ultraviolet and visible complex refractive
553 indices of secondary organic material produced by photooxidation of the aromatic compounds toluene and m-xylene,
554 *Atmospheric Chemistry and Physics*, 15, 1435-1446, doi:10.5194/acp-15-1435-2015, 2015c.

555 Makra, L., Matyasovszky, I., Guba, Z., Karatzas, K., and Anttila, P.: Monitoring the long-range transport effects on urban
556 PM10 levels using 3D clusters of backward trajectories, *Atmospheric Environment*, 45, 2630-2641,
557 doi:10.1016/j.atmosenv.2011.02.068, 2011.

558 Middlebrook, A. M., Bahreini, R., Jimenez, J. L., and Canagaratna, M. R.: Evaluation of Composition-Dependent Collection
559 Efficiencies for the Aerodyne Aerosol Mass Spectrometer using Field Data, *Aerosol Science and Technology*, 46, 258-271,
560 10.1080/02786826.2011.620041, 2012.

561 Mohr, C., DeCarlo, P. F., Heringa, M. F., Chirico, R., Slowik, J. G., Richter, R., Reche, C., Alastuey, A., Querol, X., Seco, R.,
562 Penuelas, J., Jimenez, J. L., Crippa, M., Zimmermann, R., Baltensperger, U., and Prevot, A. S. H.: Identification and
563 quantification of organic aerosol from cooking and other sources in Barcelona using aerosol mass spectrometer data,
564 *Atmospheric Chemistry and Physics*, 12, 1649-1665, doi:10.5194/acp-12-1649-2012, 2012.

565 Nakayama, T., Sato, K., Matsumi, Y., Imamura, T., Yamazaki, A., and Uchiyama, A.: Wavelength and NO_x dependent complex
566 refractive index of SOAs generated from the photooxidation of toluene, *Atmospheric Chemistry and Physics*, 13, 531-545,
567 doi:10.5194/acp-13-531-2013, 2013.

568 Ng, N. L., Kwan, A. J., Surratt, J. D., Chan, A. W. H., Chhabra, P. S., Sorooshian, A., Pye, H. O. T., Crounse, J. D., Wennberg,
569 P. O., Flagan, R. C., and Seinfeld, J. H.: Secondary organic aerosol (SOA) formation from reaction of isoprene with nitrate
570 radicals (NO₃), *Atmospheric Chemistry and Physics*, 8, 4117-4140, doi:10.5194/acp-8-4117-2008, 2008.

571 Paatero, P. and Tapper, U.: POSITIVE MATRIX FACTORIZATION - A NONNEGATIVE FACTOR MODEL WITH
572 OPTIMAL UTILIZATION OF ERROR-ESTIMATES OF DATA VALUES, *Environmetrics*, 5, 111-126,
573 doi:10.1002/env.3170050203, 1994.

574 Pachon, J. E., Weber, R. J., Zhang, X., Mulholland, J. A., and Russell, A. G.: Revising the use of potassium (K) in the source
575 apportionment of PM_{2.5}, *Atmospheric Pollution Research*, 4, 14-21, doi:10.5094/apr.2013.002, 2013.

576 Palm, B. B., Peng, Q., Fredrickson, C. D., Lee, B. H., Garofalo, L. A., Pothier, M. A., Kreidenweis, S. M., Farmer, D. K.,
577 Pokhrel, R. P., Shen, Y., Murphy, S. M., Permar, W., Hu, L., Campos, T. L., Hall, S. R., Ullmann, K., Zhang, X., Flocke, F.,

578 Fischer, E. V., and Thornton, J. A.: Quantification of organic aerosol and brown carbon evolution in fresh wildfire plumes,
579 Proceedings of the National Academy of Sciences of the United States of America, 117, 29469-29477,
580 doi:10.1073/pnas.2012218117, 2020.

581 Qin, Y. M., Tan, H. B., Li, Y. J., Li, Z. J., Schurman, M. I., Liu, L., Wu, C., and Chan, C. K.: Chemical characteristics of brown
582 carbon in atmospheric particles at a suburban site near Guangzhou, China, Atmos. Chem. Phys., 18, 16409-16418,
583 10.5194/acp-18-16409-2018, 2018.

584 Rizzo, L. V., Artaxo, P., Mueller, T., Wiedensohler, A., Paixao, M., Cirino, G. G., Arana, A., Swietlicki, E., Roldin, P., Fors, E.
585 O., Wiedemann, K. T., Leal, L. S. M., and Kulmala, M.: Long term measurements of aerosol optical properties at a primary
586 forest site in Amazonia, Atmospheric Chemistry and Physics, 13, 2391-2413, doi:10.5194/acp-13-2391-2013, 2013.

587 Rollins, A. W., Browne, E. C., Min, K. E., Pusede, S. E., Wooldridge, P. J., Gentner, D. R., Goldstein, A. H., Liu, S., Day, D.
588 A., Russell, L. M., and Cohen, R. C.: Evidence for NO_x Control over Nighttime SOA Formation, Science, 337, 1210-1212,
589 doi:10.1126/science.1221520, 2012.

590 Satish, R. and Rastogi, N.: On the Use of Brown Carbon Spectra as a Tool to Understand Their Broader Composition and
591 Characteristics: A Case Study from Crop-residue Burning Samples, Acs Omega, 4, 1847-1853,
592 doi:10.1021/acsomega.8b02637, 2019.

593 Satish, R., Shamjad, P., Thamban, N., Tripathi, S., and Rastogi, N.: Temporal Characteristics of Brown Carbon over the Central
594 Indo-Gangetic Plain, Environmental Science & Technology, 51, 6765-6772, doi:10.1021/acs.est.7b00734, 2017.

595 Schnitzler, E. G., Liu, T., Hems, R. F., and Abbatt, J. P. D.: Emerging investigator series: heterogeneous OH oxidation of
596 primary brown carbon aerosol: effects of relative humidity and volatility, Environmental Science-Processes & Impacts, 22,
597 2162-2171, doi:10.1039/d0em00311e, 2020.

598 Schuetzle, D.: SAMPLING OF VEHICLE EMISSIONS FOR CHEMICAL-ANALYSIS AND BIOLOGICAL TESTING,
599 Environmental Health Perspectives, 47, 65-80, doi:10.2307/3429500, 1983.

600 Schwarz, J. P., Spackman, J. R., Fahey, D. W., Gao, R. S., Lohmann, U., Stier, P., Watts, L. A., Thomson, D. S., Lack, D. A.,
601 Pfister, L., Mahoney, M. J., Baumgardner, D., Wilson, J. C., and Reeves, J. M.: Coatings and their enhancement of black carbon
602 light absorption in the tropical atmosphere, Journal of Geophysical Research-Atmospheres, 113, doi:10.1029/2007jd009042,
603 2008.

604 Shen, G., Ru, M., Du, W., Zhu, X., Zhong, Q., Chen, Y., Shen, H., Yun, X., Meng, W., Liu, J., Cheng, H., Hu, J., Guan, D., and
605 Tao, S.: Impacts of air pollutants from rural Chinese households under the rapid residential energy transition, Nature
606 Communications, 10, doi:10.1038/s41467-019-11453-w, 2019.

607 Siemens, K., Morales, A., He, Q., Li, C., Hettiyadura, A. P. S., Rudich, Y., and Laskin, A.: Molecular Analysis of Secondary
608 Brown Carbon Produced from the Photooxidation of Naphthalene, Environmental science & technology, 56, 3340-3353,
609 doi:10.1021/acs.est.1c03135, 2022.

610 Sun, Y., Jiang, Q., Wang, Z., Fu, P., Li, J., Yang, T., and Yin, Y.: Investigation of the sources and evolution processes of severe
611 haze pollution in Beijing in January 2013, Journal of Geophysical Research-Atmospheres, 119, 4380-4398,

612 doi:10.1002/2014jd021641, 2014.

613 Sun, Y., Du, W., Fu, P., Wang, Q., Li, J., Ge, X., Zhang, Q., Zhu, C., Ren, L., Xu, W., Zhao, J., Han, T., Worsnop, D. R., and
614 Wang, Z.: Primary and secondary aerosols in Beijing in winter: sources, variations and processes, *Atmos Chem Phys*, 16, 8309-
615 8329, doi:10.5194/acp-16-8309-2016, 2016.

616 Sun, Y. L., Zhang, Q., Schwab, J. J., Chen, W. N., Bae, M. S., Lin, Y. C., Hung, H. M., and Demerjian, K. L.: A case study of
617 aerosol processing and evolution in summer in New York City, *Atmos Chem Phys*, 11, 12737-12750, doi:10.5194/acp-11-
618 12737-2011, 2011a.

619 Sun, Y. L., Zhang, Q., Schwab, J. J., Demerjian, K. L., Chen, W. N., Bae, M. S., Hung, H. M., Hogrefe, O., Frank, B., Rattigan,
620 O. V., and Lin, Y. C.: Characterization of the sources and processes of organic and inorganic aerosols in New York city with a
621 high-resolution time-of-flight aerosol mass spectrometer, *Atmospheric Chemistry and Physics*, 11, 1581-1602,
622 doi:10.5194/acp-11-1581-2011, 2011b.

623 Taylor, J. W., Allan, J. D., Liu, D., Flynn, M., Weber, R., Zhang, X., Lefer, B. L., Grossberg, N., Flynn, J., and Coe, H.:
624 Assessment of the sensitivity of core/shell parameters derived using the single-particle soot photometer to density and
625 refractive index, *Atmospheric Measurement Techniques*, 8, 1701-1718, doi:10.5194/amt-8-1701-2015, 2015.

626 Tian, P., Liu, D., Zhao, D., Yu, C., Liu, Q., Huang, M., Deng, Z., Ran, L., Wu, Y., Ding, S., Hu, K., Zhao, G., Zhao, C., and
627 Ding, D.: In situ vertical characteristics of optical properties and heating rates of aerosol over Beijing, *Atmospheric Chemistry
628 and Physics*, 20, 2603-2622, doi:10.5194/acp-20-2603-2020, 2020.

629 Ulbrich, I. M., Canagaratna, M. R., Zhang, Q., Worsnop, D. R., and Jimenez, J. L.: Interpretation of organic components from
630 Positive Matrix Factorization of aerosol mass spectrometric data, *Atmospheric Chemistry and Physics*, 9, 2891-2918,
631 doi:10.5194/acp-9-2891-2009, 2009.

632 Updyke, K. M., Nguyen, T. B., and Nizkorodov, S. A.: Formation of brown carbon via reactions of ammonia with secondary
633 organic aerosols from biogenic and anthropogenic precursors, *Atmospheric Environment*, 63, 22-31,
634 doi:10.1016/j.atmosenv.2012.09.012, 2012.

635 Wang, J., Ye, J., Zhang, Q., Zhao, J., Wu, Y., Li, J., Liu, D., Li, W., Zhang, Y., Wu, C., Xie, C., Qin, Y., Lei, Y., Huang, X., Guo,
636 J., Liu, P., Fu, P., Li, Y., Lee, H. C., Choi, H., Zhang, J., Liao, H., Chen, M., Sun, Y., Ge, X., Martin, S. T., and Jacob, D. J.:
637 Aqueous production of secondary organic aerosol from fossil-fuel emissions in winter Beijing haze, *Proceedings of the
638 National Academy of Sciences*, 118, e2022179118, doi:10.1073/pnas.2022179118, 2021.

639 Wang, Q., Liu, H., Wang, P., Dai, W., Zhang, T., Zhao, Y., Tian, J., Zhang, W., Han, Y., and Cao, J.: Optical source
640 apportionment and radiative effect of light-absorbing carbonaceous aerosols in a tropical marine monsoon climate zone: the
641 importance of ship emissions, *Atmos Chem Phys*, 20, 15537-15549, doi:10.5194/acp-20-15537-2020, 2020.

642 Wang, Q., Han, Y., Ye, J., Liu, S., Pongpiachan, S., Zhang, N., Han, Y., Tian, J., Wu, C., Long, X., Zhang, Q., Zhang, W., Zhao,
643 Z., and Cao, J.: High Contribution of Secondary Brown Carbon to Aerosol Light Absorption in the Southeastern Margin of
644 Tibetan Plateau, *Geophysical Research Letters*, 46, 4962-4970, doi:10.1029/2019gl082731, 2019a.

645 Wang, Q., Cao, J., Han, Y., Tian, J., Zhang, Y., Pongpiachan, S., Zhang, Y., Li, L., Niu, X., Shen, Z., Zhao, Z., Tipmanee, D.,

646 Bunsomboonsakul, S., Chen, Y., and Sun, J.: Enhanced light absorption due to the mixing state of black carbon in fresh biomass
647 burning emissions, *Atmospheric Environment*, 180, 184-191, doi:10.1016/j.atmosenv.2018.02.049, 2018a.

648 Wang, Q., Ye, J., Wang, Y., Zhang, T., Ran, W., Wu, Y., Tian, J., Li, L., Zhou, Y., Hang Ho, S. S., Dang, B., Zhang, Q., Zhang,
649 R., Chen, Y., Zhu, C., and Cao, J.: Wintertime Optical Properties of Primary and Secondary Brown Carbon at a Regional Site
650 in the North China Plain, *Environmental Science & Technology*, 53, 12389-12397, 10.1021/acs.est.9b03406, 2019b.

651 Wang, Q., Ye, J., Wang, Y., Zhang, T., Ran, W., Wu, Y., Tian, J., Li, L., Zhou, Y., Ho, S. S. H., Dang, B., Zhang, Q., Zhang, R.,
652 Chen, Y., Zhu, C., and Cao, J.: Wintertime Optical Properties of Primary and Secondary Brown Carbon at a Regional Site in
653 the North China Plain, *Environmental Science & Technology*, 53, 12389-12397, 10.1021/acs.est.9b03406, 2019c.

654 Wang, X., Heald, C. L., Liu, J., Weber, R. J., Campuzano-Jost, P., Jimenez, J. L., Schwarz, J. P., and Perring, A. E.: Exploring
655 the observational constraints on the simulation of brown carbon, *Atmos Chem Phys*, 18, 635-653, doi:10.5194/acp-18-635-
656 2018, 2018b.

657 Wang, X., Heald, C. L., Ridley, D. A., Schwarz, J. P., Spackman, J. R., Perring, A. E., Coe, H., Liu, D., and Clarke, A. D.:
658 Exploiting simultaneous observational constraints on mass and absorption to estimate the global direct radiative forcing of
659 black carbon and brown carbon, *Atmospheric Chemistry and Physics*, 14, 10989-11010, doi:10.5194/acp-14-10989-2014, 2014.

660 Wang, Y., Hu, M., Wang, Y., Zheng, J., Shang, D., Yang, Y., Liu, Y., Li, X., Tang, R., Zhu, W., Du, Z., Wu, Y., Guo, S., Wu, Z.,
661 Lou, S., Hallquist, M., and Yu, J. Z.: The formation of nitro-aromatic compounds under high NO_x and anthropogenic VOC
662 conditions in urban Beijing, China, *Atmospheric Chemistry and Physics*, 19, 7649-7665, doi:10.5194/acp-19-7649-2019,
663 2019d.

664 Wu, C. and Yu, J. Z.: Determination of primary combustion source organic carbon-to-elemental carbon (OC_{aEuro}/aEuro-EC)
665 ratio using ambient OC and EC measurements: secondary OC-EC correlation minimization method, *Atmos Chem Phys*, 16,
666 5453-5465, doi:10.5194/acp-16-5453-2016, 2016.

667 Yang, W., Zhang, Y., Wang, X., Li, S., Zhu, M., Yu, Q., Li, G., Huang, Z., Zhang, H., Wu, Z., Song, W., Tan, J., and Shao, M.:
668 Volatile organic compounds at a rural site in Beijing: influence of temporary emission control and wintertime heating,
669 *Atmospheric Chemistry and Physics*, 18, 12663-12682, doi:10.5194/acp-18-12663-2018, 2018.

670 Yao, Z., Shen, X., Ye, Y., Cao, X., Jiang, X., Zhang, Y., and He, K.: On-road emission characteristics of VOCs from diesel
671 trucks in Beijing, China, *Atmospheric Environment*, 103, 87-93, doi:10.1016/j.atmosenv.2014.12.028, 2015.

672 Zhang, Q., Worsnop, D. R., Canagaratna, M. R., and Jimenez, J. L.: Hydrocarbon-like and oxygenated organic aerosols in
673 Pittsburgh: insights into sources and processes of organic aerosols, *Atmos Chem Phys*, 5, 3289-3311, doi:10.5194/acp-5-3289-
674 2005, 2005.

675 Zhang, Q., Jimenez, J. L., Canagaratna, M. R., Ulbrich, I. M., Ng, N. L., Worsnop, D. R., and Sun, Y.: Understanding
676 atmospheric organic aerosols via factor analysis of aerosol mass spectrometry: a review, *Analytical and Bioanalytical*
677 *Chemistry*, 401, 3045-3067, doi:10.1007/s00216-011-5355-y, 2011.

678 Zhang, Q., Shen, Z., Zhang, L., Zeng, Y., Ning, Z., Zhang, T., Lei, Y., Wang, Q., Li, G., Sun, J., Westerdahl, D., Xu, H., and
679 Cao, J.: Investigation of Primary and Secondary Particulate Brown Carbon in Two Chinese Cities of Xi'an and Hong Kong in

680 Wintertime, *Environmental Science & Technology*, 54, 3803-3813, doi:10.1021/acs.est.9b05332, 2020.

681 Zhang, Y., Wang, Q., Tian, J., Li, Y., Liu, H., Ran, W., Han, Y., Prévôt, A. S. H., and Cao, J.: Impact of COVID-19 lockdown
682 on the optical properties and radiative effects of urban brown carbon aerosol, *Geoscience Frontiers*, 13, 101320,
683 10.1016/j.gsf.2021.101320, 2022.

684 Zhang, Y., Zhang, Q., Cheng, Y., Su, H., Li, H., Li, M., Zhang, X., Ding, A., and He, K.: Amplification of light absorption of
685 black carbon associated with air pollution, *Atmospheric Chemistry and Physics*, 18, 9879-9896, doi:10.5194/acp-18-9879-
686 2018, 2018.

687 Zhao, R., Lee, A. K. Y., Huang, L., Li, X., Yang, F., and Abbatt, J. P. D.: Photochemical processing of aqueous atmospheric
688 brown carbon, *Atmospheric Chemistry and Physics*, 15, 6087-6100, doi:10.5194/acp-15-6087-2015, 2015.

689 Zhou, S., Collier, S., Xu, J., Mei, F., Wang, J., Lee, Y.-N., Sedlacek, A. J., III, Springston, S. R., Sun, Y., and Zhang, Q.:
690 Influences of upwind emission sources and atmospheric processing on aerosol chemistry and properties at a rural location in
691 the Northeastern US, *Journal of Geophysical Research-Atmospheres*, 121, 6049-6065, doi:10.1002/2015jd024568, 2016.

692

693